

THE DIAGONAL TENSOR APPROXIMATION (DTA) FOR OBJECTS IN A NON-CANONICAL INHOMOGENEOUS BACKGROUND

M. Yuan and Q. H. Liu

Department of Electrical and Computer Engineering
Duke University, Durham, NC 27708, USA

Abstract—A non-canonical inhomogeneous background medium is one whose Green's function cannot be obtained by an analytical method. Electromagnetic scattering from objects embedded in a non-canonical inhomogeneous background medium is very challenging because of the computational complexity with the calculation of its Green's function and the multiple scattering between objects and the background. This work applies the Diagonal Tensor Approximation (DTA) to calculate the scattering from arbitrary objects in a non-canonical inhomogeneous background. Previously, the DTA has only been applied to a canonical background such as a homogeneous or layered background media. This approach employs a numerical method to obtain all Green's functions required in the calculation; an accurate DTA is used to calculate the scattering properties. In order to reduce the large number of simulations, we employ the symmetry and reciprocity in the Green's function calculation. Furthermore, considering that most realistic imaging measurements are made through a voltage probe usually represented by a wave port, we develop a method to convert the scattered field on the probe (the antenna) to the measured wave port voltage. Numerical results show that this method can obtain accurate scattering characteristics from arbitrary objects in a non-canonical inhomogeneous background medium in a microwave imaging system.

1. INTRODUCTION

Over the past years, there have been growing interests in the electromagnetic scattering problem for biomedical applications. Various methods, such as the finite-element method (FEM), method of moments (MOM) [1], and finite-difference time-domain (FDTD) method have been applied as full-wave solution techniques; and the Born approximation [2] have been proposed and implemented as an approximate method. But these methods have their limitations, especially for objects embedded in a complex background medium. Although the full-wave methods can provide accurate results, they need to solve a large system matrix (FEM and MOM) or require large number of time steps (FDTD). It is therefore usually too expensive for a realistic 3D biomedical imaging system. For example, in the MOM, in order to obtain the scattered field, we need to solve the current distribution in the computation domain, which normally needs $O(N^3)$ CPU time (N is the number of unknowns) if a direct matrix inversion method is used. The Born approximation is a fast method to solve the scattering without the inversion of a system matrix, but it is valid for weak scattering only. The accuracy of the Born approximation decreases rapidly with the increasing target contrast and size. Several improved Born approximation methods have been proposed to overcome the weak scattering limitations, for example, the extended Born approximation (EBA) [3, 4], the quasi-linear (QL) or quasi-analytical (QA) approximation [5–7], and the Diagonal Tensor Approximation (DTA) [8, 9]. Normally these methods need only $O(N^2)$ CPU time to obtain the current distribution in the computation domain; furthermore, $O(N \log N)$ algorithms have been developed for homogeneous and layered background media [10]. The performance of these improved approximations under higher contrasts has been verified by [11–13, 19–22], and some of these methods have been employed in inverse problems [14–22, 27–31]. These improved approximations are successful methods for the forward and inverse modeling and they have been compared in [8, 9].

Up to date, however, due to the complexity of the scattering problem in an arbitrary inhomogeneous background, the reported research on the improved Born approximations have so far been applied to a canonical background medium, for example, a homogenous medium or a layered medium background, whose Green's function can be obtained analytically. Meanwhile, the interferences from antennas (probes) are usually ignored in all previous approximations. But these presuppositions will limit the application range. In order to overcome these limitations, in this paper, we propose a strategy to build the

system matrix for an arbitrary non-canonical background medium with arbitrary type of probes; here, we define a non-canonical background as one that has an inhomogeneous background medium whose Green's function cannot be obtained analytically. This also allows the inclusion of the coupling from antennas in the system. Through this method, we can develop the improved Born approximations to a more complicated background and thus widen the application range.

We focus our efforts on a fixed biomedical imaging system whose sensors (antennas) is one fixed configuration, thus the system response can be repeatedly used in the forward and inverse simulations. For such a fixed scattering measurement system, in an approximation method, we can assume the Green's function for the background medium in this system is fixed. When a target is placed into the system, the total electric field can be solved by the DTA method with the known background Green's function, then the scattering from targets can be solved by the total electric field. Basing on this assumption, we can pre-calculate and save the system Green's function before solving the problem. With the fast development of numerical EM methods and the computer technology, many EM solvers are available and can solve the forward problem with high accuracy. In this paper, we propose a strategy to implement the DTA method in a non-canonical background medium: pre-calculating the Green's function numerically. Although this pre-calculation might be expensive, it is a one-time simulation; thus the method is effective for a fixed measurement system such as a microwave imager. If the scattering measurement system is fixed, the cost on pre-calculation becomes negligible for a long term usage.

In this research, we use a commercial software Wavenology EM to solve the Green's function. Due to the large number of Green's functions needed to be solved, the method of taking advantage of the symmetry of the measurement system and the reciprocity property of the Green's function to reduce the number of simulation cases is investigated. Furthermore, considering that the realistic measurement normally is the voltage on the probe feeding structure, we further develop a method to convert the scattered field to measured voltage.

This paper is organized as follows: Section 2 presents a brief description of the Green's function calculation method, the DTA method, the reciprocity of the Green's function, converting the scattered field to measured voltage, and the scheme of taking advantage of the symmetry of the measurement system to reduce the number of simulation cases. Section 3 presents the numerical results, including the validation of the reciprocity of the Green's function in a numerical method and accuracy of scattering using the DTA method. Section 4 is the conclusion.

2. THEORY

Figure 1 shows a general scattering measurement system in a microwave imager with printed circuit boards and antennas mounted on the boards. Some examples are a rectangular PCB chamber, where probes are patch antennas fabricated on the chamber walls [23–25]. The computation domain is the center region of the chamber, and the measurement is the S_{21} at the antennas. Normally, the chamber is filled with a background material to reduce the scattering from the target surface. Obviously, this is a measurement system with a non-canonical inhomogeneous background medium. The electromagnetic scattering of objects inside this chamber will be investigated by the DTA.

2.1. The Scattering Problem

In a complicated 3-D problems shown in Fig. 1, the time-harmonic scattered electric field (with $e^{j\omega t}$ time convention) at an observer can be expressed by the volume equivalence principle

$$\mathbf{E}^{sct}(\mathbf{r}) = -j\omega\tilde{\mu}_b \int_D \mathbf{G}(\mathbf{r}, \mathbf{r}') \cdot \mathbf{J}(\mathbf{r}') d\mathbf{r}' = \tilde{k}_b^2 \int_D \mathbf{G}(\mathbf{r}, \mathbf{r}') \cdot \chi(\mathbf{r}') \mathbf{E}(\mathbf{r}') d\mathbf{r}' \quad (1)$$

where $\tilde{\mu}_b$ is the complex permeability of the background. $\mathbf{J} = j\omega(\tilde{\epsilon} - \tilde{\epsilon}_b)\mathbf{E}$ is the induced current density in the object, $\tilde{\epsilon} = \epsilon_0\epsilon_r - j\sigma/\omega$ is the object complex permittivity (ϵ_r is the relative dielectric constant of object, ϵ_0 is the permittivity of free space, σ is the conductivity of object), and $\tilde{\epsilon}_b$ is the complex permittivity of the background. \mathbf{E} is the total field in the computation domain, $\chi(\mathbf{r}')$ is a contrast value defined as $\chi(\mathbf{r}') = \tilde{\epsilon}(\mathbf{r}')/\tilde{\epsilon}_b(\mathbf{r}') - 1$, and $\mathbf{G}(\mathbf{r}, \mathbf{r}')$ is a dyadic Green's function from a source point at \mathbf{r}' to the observer at \mathbf{r} in a non-

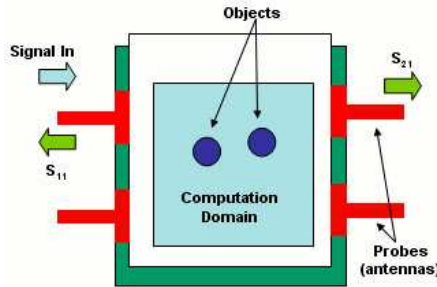


Figure 1. A microwave imaging system with printed circuit boards and antennas mounted on the boards.

canonical inhomogeneous background. D is the computation domain, and $\tilde{k}_b^2 = \omega^2 \tilde{\epsilon}_b \tilde{\mu}_b$.

According to (1), to obtain the scattered field, the dyadic Green's function $\mathbf{G}(\mathbf{r}, \mathbf{r}')$ and the total field in the computation domain \mathbf{E} must be solved first. Normally this is done with the MOM by solving the volume integral equation in the computation domain. However, this is an expensive method to use in terms of both memory and CPU time requirements. In our work, we use the DTA method to calculate \mathbf{E} , and use a numerical method combined with reciprocity theorem to obtain the dyadic Green's function $\mathbf{G}(\mathbf{r}, \mathbf{r}')$.

2.2. The Diagonal Tensor Approximation (DTA)

To reduce the computational costs from the MOM, here we apply the Diagonal Tensor Approximation [8, 9] to solve the scattering problem for objects in a non-canonical inhomogeneous background medium. For this purpose, the total field \mathbf{E} in Equation (1) inside the computation domain can be expressed as

$$\mathbf{E}(\mathbf{r}) = \mathbf{E}^{inc}(\mathbf{r}) + \mathbf{E}^{sct}(\mathbf{r}) = \mathbf{E}^{inc}(\mathbf{r}) + \tilde{k}_b^2 \int_D \mathbf{G}(\mathbf{r}, \mathbf{r}') \cdot \chi(\mathbf{r}') \mathbf{E}(\mathbf{r}') d\mathbf{r}' \quad (2)$$

where $\mathbf{E}^{inc}(\mathbf{r})$ is the incident field, which can be obtained from a numerical method for a non-canonical inhomogeneous background medium.

In the DTA method, $\mathbf{E}(\mathbf{r}')$ inside the object can be approximated by

$$\mathbf{E}(\mathbf{r}') \approx [\mathbf{I} + \mathbf{\Gamma}(\mathbf{r}')] \cdot \mathbf{E}^{inc}(\mathbf{r}') \quad (3)$$

where $\mathbf{\Gamma}(\mathbf{r}')$ is a diagonal scattering tensor

$$\mathbf{\Gamma} \approx \begin{bmatrix} \gamma_x & 0 & 0 \\ 0 & \gamma_y & 0 \\ 0 & 0 & \gamma_z \end{bmatrix} \quad (4)$$

that is used to approximate the full scattering tensor. This approximate tensor $\mathbf{\Gamma}(\mathbf{r}')$ can be calculated by [8]

$$[\gamma_x \ \gamma_y \ \gamma_z]^T = \left\{ \text{diag} [\mathbf{E}^{inc}(\mathbf{r}')] - \mathbf{G}^b(\mathbf{r}') \right\}^{-1} \cdot \mathbf{E}^b(\mathbf{r}') \quad (5)$$

where

$$\text{diag} [\mathbf{E}^{inc}(\mathbf{r}')] = \begin{bmatrix} E_x^{inc}(\mathbf{r}') & 0 & 0 \\ 0 & E_y^{inc}(\mathbf{r}') & 0 \\ 0 & 0 & E_z^{inc}(\mathbf{r}') \end{bmatrix} \quad (6)$$

$$\mathbf{E}^b(\mathbf{r}') = \tilde{k}_b^2 \int_D \mathbf{G}(\mathbf{r}', \mathbf{r}'') \cdot \chi(\mathbf{r}'') \mathbf{E}^{inc}(\mathbf{r}'') d\mathbf{r}'' \quad (7)$$

$$\mathbf{G}^b(\mathbf{r}') = \begin{bmatrix} g_{xx}(\mathbf{r}') & g_{xy}(\mathbf{r}') & g_{xz}(\mathbf{r}') \\ g_{yx}(\mathbf{r}') & g_{yy}(\mathbf{r}') & g_{yz}(\mathbf{r}') \\ g_{zx}(\mathbf{r}') & g_{zy}(\mathbf{r}') & g_{zz}(\mathbf{r}') \end{bmatrix} \quad (8)$$

In the above,

$$g_{ij}(\mathbf{r}') = \tilde{k}_b^2 \int_D G_{ij}(\mathbf{r}', \mathbf{r}'') \cdot \chi(\mathbf{r}'') E_j^{inc}(\mathbf{r}'') d\mathbf{r}'' \quad (9)$$

where $i, j = x, y, z$, $G_{ij}(\mathbf{r}', \mathbf{r}'')$ is the ij th component of the dyadic Green's function for an ideal electric dipole source in a non-canonical inhomogeneous background. Similar to the incident field, this dyadic Green's function normally has to be obtained numerically due to the presence of a non-canonical inhomogeneous background.

After the total field inside the object is approximated by the DTA, a numerical integration of the dyadic Green's function operating on the induced electric current density can be performed to arrive at the electric field at an observer. For simplicity, we will discretize (2) to obtain the electric field as

$$\mathbf{E}(\mathbf{r}_i) = \mathbf{E}^{inc}(\mathbf{r}_i) + \tilde{k}_b^2 \sum_{j=1}^N \mathbf{G}(\mathbf{r}_i, \mathbf{r}_j) \cdot \chi(\mathbf{r}_j) \mathbf{E}(\mathbf{r}_j) \Delta V_j \quad (10)$$

where \mathbf{r}_j is the j th cell center position, $\mathbf{G}(\mathbf{r}_i, \mathbf{r}_j)$ is the dyadic Green's function from a current at j th cell to the observer at i th cell, and ΔV_j is the volume of the j -th cell.

Normally, it is impossible to obtain $\mathbf{G}(\mathbf{r}_i, \mathbf{r}_j)$ analytically for a non-canonical inhomogeneous background. Considering current numerical EM solvers can provide accurate results, in this work, we use a numerical method combined with the reciprocity theorem to solve for the dyadic Green's function.

2.3. Reciprocity for the Green's Function

In order to calculate scattered field $\mathbf{E}^{sct}(\mathbf{r})$, we need to know the dyadic Green's function $\mathbf{G}(\mathbf{r}, \mathbf{r}')$ to solve (2). Because of the presence of an inhomogeneous background medium, this dyadic Green's function will be obtain numerically.

If the fields produced by electric current sources $\mathbf{J}_i(\mathbf{r})$ and $\mathbf{J}_j(\mathbf{r})$ are denoted by $\mathbf{E}_i(\mathbf{r})$ and $\mathbf{E}_j(\mathbf{r})$ respectively, then according to the reciprocity theorem, we have

$$\int_D \mathbf{J}_i(\mathbf{r}) \cdot \mathbf{E}_j(\mathbf{r}) d\mathbf{r} = \int_D \mathbf{J}_j(\mathbf{r}) \cdot \mathbf{E}_i(\mathbf{r}) d\mathbf{r} \quad (11)$$

Choosing these sources as point dipoles $\mathbf{J}_i = \hat{a}_i \delta(\mathbf{r} - \mathbf{r}_i)$, and $\mathbf{J}_j = \hat{a}_j \delta(\mathbf{r} - \mathbf{r}_j)$ where \hat{a}_i and \hat{a}_j are the dipole directions, we obtain

$$\int_D [\hat{a}_i \delta(\mathbf{r} - \mathbf{r}_i)] \cdot \mathbf{E}_j(\mathbf{r}) d\mathbf{r} = \int_D [\hat{a}_j \delta(\mathbf{r} - \mathbf{r}_j)] \cdot \mathbf{E}_i(\mathbf{r}) d\mathbf{r} \quad (12)$$

or

$$\hat{a}_i \cdot \mathbf{G}(\mathbf{r}_i, \mathbf{r}_j) \cdot \hat{a}_j = \hat{a}_j \cdot \mathbf{G}(\mathbf{r}_j, \mathbf{r}_i) \cdot \hat{a}_i \quad (13)$$

Therefore,

$$\mathbf{G}(\mathbf{r}_i, \mathbf{r}_j) = [\mathbf{G}(\mathbf{r}_j, \mathbf{r}_i)]^T \quad (14)$$

according to the reciprocity theorem for an arbitrary inhomogeneous background medium.

2.4. Use of Symmetry to Reduce the Number of Simulations

To approximate the total electric field inside the object in DTA by Equation (10), the dyadic Green's function is needed for sources located at every cell. This precalculation can be time consuming. However, symmetry of the problem geometry can be explored to reduce the number of numerical simulations needed for this dyadic Green's function.

Theoretically, in order to solve (10), we need to run N simulations (N is the total number of cells) to obtain the Green's functions from N sources to N receivers. For each simulation, there is an ideal electric dipole source at the i th cell center and N point probes at all cell centers. But if the measurement system is symmetric as in typical microwave imaging systems (such as that in [25]), for example, as the rectangular chamber used in Fig. 5, which is symmetric along $x = y$, $x = 0$, $y = 0$ planes respectively, we only need to simulate about $N/8$ cases, then use the symmetry to obtain N^2 Green's functions.

Here, we use a 2D case to show our scheme of using the symmetry and reciprocity together. As shown in Fig. 2, there are 16 cells in the object domain, and the system is symmetric along the $x = y$, $x = 0$ and $y = 0$ planes respectively. In the first step, we need to place an point dipole source at cells 11, 12 and 16, respectively to get the Green's function from source cells 11, 12 and 16 to all cells. Because the system is symmetric along $x = y$ plane, we can obtain the Green's function from cell 15 to all cells by mirroring the results for source at cell 12 about the $x = y$ plane. Then, we can obtain the Green's function from source cells 9, 10, 13 and 14 by mirroring the results for source cells 11, 12, 15 and 16 about the $x = 0$ plane. Finally, in the same way we obtain the Green's function for source cells 1–8. Through

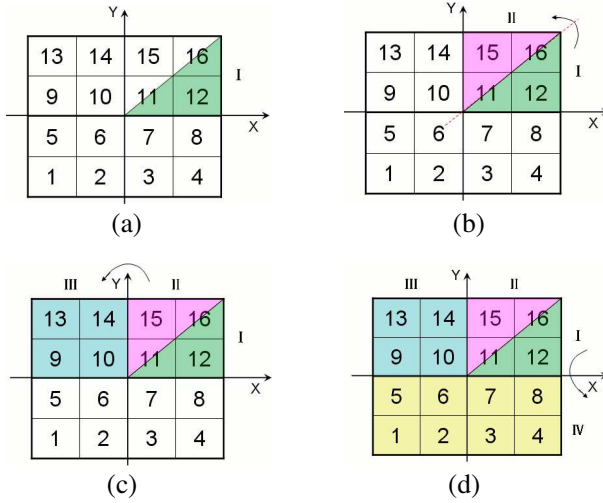


Figure 2. (a) Simulate the cases with source at cell 11, 12, 16, respectively. (b) Obtain the Green's function for source at cell 15 by mirroring along $x = y$ plane. (c) Obtain the Green's function for source at cell 9, 10, 13 and 14 by mirroring along $x = 0$ plane. (d) Obtain the Green's function for source at cell 1–8 by mirroring along $y = 0$ plane.

this scheme, we need only 3 simulations, instead of 16 simulations, to obtain the 16×16 Green's functions. Similarly, for a 3D system with 2D symmetry with respect to $x = y$, $x = 0$ and $y = 0$ planes, the total simulation requirement will be significantly reduced by a factor about 8 (through above steps, $y = 0$ symmetry can reduce the number of simulation cases by half; $x = 0$ symmetry can further half the number of simulation cases; finally, $x = y$ symmetry can reduce the number of simulation cases by about half; therefore, the factor is approximately $2 \times 2 \times 2 = 8$).

2.5. The Green's Function from Object Domain to a Receiver

Once the electric field has been found by the DTA inside the object domain discretized by N cells, the electric field at a receiver at \mathbf{r} can be found from (1). To do this, we need to know Green's function $\mathbf{G}(\mathbf{r}, \mathbf{r}')$ for sources at the N cells inside the object domain to the receiver. This requires N numerical simulations. But according to the reciprocity theorem in Equation (14), if we can obtain this by the transpose of $\mathbf{G}(\mathbf{r}', \mathbf{r})$, i.e., the Green's function from a source at the

receiver location to all cells in the object domain. Thus, the total simulation requirement will be significantly reduced by a factor of N for one receiver outside the object. If there are N_R receivers, the saving factor will be N/N_R .

2.6. The Wave Port Green's Function \mathbf{G}_u

In a realistic system, the receiving probes are usually not ideal point electric dipoles as described in the last subsection, but wave ports to characterize the antenna feeding ports. The measured data are usually the wave port voltage values (or the S parameters if voltages are normalized) at these antenna feeding ports. Here, we derive the relationship between the wave port voltage and the scattered field from the object on the wave port.

Assume that an antenna is fed by a wave port with a port area S , and the object is located at $\mathbf{r} \in D$ outside the antenna. We setup two cases: In case 1, we have an induced electric current density \mathbf{J} inside a volume D in the inhomogeneous background medium, and the scattered voltage response V on wave port is calculated through \mathbf{E}^{sct} and \mathbf{H}^{sct} radiated by this induced source; in case 2, we excite the antenna with a waveport and obtain the electric field response at $\mathbf{r} \in D$. We will derive the reciprocity relation for the voltage and electric and magnetic fields.

We define the electric and magnetic fields for the guided mode in the wave port as \mathbf{e}_m and \mathbf{h}_m . Here we assumed that \mathbf{e}_m and \mathbf{h}_m have been already normalized. Then in case 1 where an induced electric current density $\mathbf{J}(\mathbf{r})$ for $\mathbf{r} \in D$, according to [26], the voltage on a wave port as a receiver can be obtained by

$$\int_S \{ \mathbf{E}^{sct}(\mathbf{r}) \times [-\mathbf{h}_m(\mathbf{r})] \} \cdot \hat{n} ds = V, \quad (15)$$

where \mathbf{E}^{sct} is the scattered electric field response on the wave port due to the induced electric current source in D , and \hat{n} is the outward normal of the wave port surface. Equation (15) can be rewritten as

$$\begin{aligned} V &= \int_S [-\mathbf{h}_m(\mathbf{r}) \times \hat{n}] \cdot \mathbf{E}^{sct}(\mathbf{r}) ds = \int_D \int_S ds [\hat{n} \times \mathbf{h}_m(\mathbf{r})] \cdot \mathbf{G}(\mathbf{r}, \mathbf{r}') \cdot \mathbf{J}(\mathbf{r}') d\mathbf{r}' \\ &= \int_D \mathbf{G}_u(\mathbf{r}, \mathbf{r}') \cdot \mathbf{J}(\mathbf{r}') d\mathbf{r}' \end{aligned} \quad (16)$$

where the vector Green's function

$$\mathbf{G}_u(\mathbf{r}, \mathbf{r}') = \int_S [\hat{n} \times \mathbf{h}_m(\mathbf{r})] \cdot \mathbf{G}(\mathbf{r}, \mathbf{r}') ds \quad (17)$$

can be obtained by a numerical method.

2.7. Reciprocity for the Wave Port Green's Function

Now, we are ready to discuss the two cases and their reciprocity relationship: In case 1, we have an induced electric current density \mathbf{J}_1 inside a volume D in the inhomogeneous background medium, and the scattered voltage response V on wave port is calculated through \mathbf{E}^{sct} and \mathbf{H}^{sct} radiated by this induced source; in case 2, we excite the antenna with a wave port mode and obtain the electromagnetic field response \mathbf{E}_2 and \mathbf{H}_2 at $\mathbf{r} \in D$. We will derive the reciprocity relation for the voltage and electric and magnetic fields.

In case 1, the induced electric current source $\mathbf{J}_1(\mathbf{r})$ for $\mathbf{r} \in D$ produces electric field \mathbf{E}_1 and magnetic field \mathbf{H}_1 in wave port S .

In case 2, for a wave port source at feeding position S , the equivalent currents corresponding to the m -th mode of as the incident field in the port can be expressed as

$$\mathbf{J}_2(\mathbf{r}) = -\hat{n} \times \mathbf{h}_m(\mathbf{r}); \quad \mathbf{M}_2(\mathbf{r}) = \hat{n} \times \mathbf{e}_m(\mathbf{r}), \quad \mathbf{r} \in S \quad (18)$$

where $\mathbf{h}_m(\mathbf{r})$ and $\mathbf{e}_m(\mathbf{r})$ are the incident electric and magnetic fields in the wave port for an inward propagating mode respectively. This wave port excitation produces an electric field \mathbf{E}_2 at $\mathbf{r} \in D$, which is outside the wave port surface S .

According to the reciprocity theorem, we have

$$\int_S [\mathbf{J}_2(\mathbf{r}) \cdot \mathbf{E}_1(\mathbf{r}) - \mathbf{M}_2(\mathbf{r}) \cdot \mathbf{H}_1(\mathbf{r})] ds = \int_D \mathbf{J}_1(\mathbf{r}) \cdot \mathbf{E}_2(\mathbf{r}) d\mathbf{r} \quad (19)$$

and

$$\int_S [-\hat{n} \times \mathbf{h}_m(\mathbf{r}) \cdot \mathbf{E}_1(\mathbf{r}) - \hat{n} \times \mathbf{e}_m(\mathbf{r}) \cdot \mathbf{H}_1(\mathbf{r})] ds = \int_D \mathbf{J}_1(\mathbf{r}) \cdot \mathbf{E}_2(\mathbf{r}) d\mathbf{r} \quad (20)$$

As the normalized voltage and current on a wave port can be defined as [26]

$$V = \int_S \{\mathbf{E}_1(\mathbf{r}) \times [-\mathbf{h}_{tm}(\mathbf{r})]\} \cdot \hat{n} ds; \quad I = \int_S [\mathbf{e}_{tm}(\mathbf{r}) \times \mathbf{H}_1(\mathbf{r})] \cdot \hat{n} ds, \quad (21)$$

where \mathbf{e}_{tm} and \mathbf{h}_{tm} are the transverse field distributions of the m -th waveguide mode propagating into the wave port, Equation (19) can be rewritten as

$$V + I = \int_D \mathbf{J}_1(\mathbf{r}) \cdot \mathbf{E}_2(\mathbf{r}) d\mathbf{r} \quad (22)$$

In the special case, where the current density \mathbf{J}_1 is a point dipole, i.e., $\mathbf{J}_1 = \hat{a}\delta(\mathbf{r} - \mathbf{r}_1)$, we have

$$V + I = \hat{a} \cdot \mathbf{E}_2(\mathbf{r}_1) \quad (23)$$

Therefore, the electric response of a wave port source is equal to the summation of the normalized voltage and current responses on the port due to an electric dipole source.

3. NUMERICAL RESULTS

3.1. Verification of the Reciprocity of an Ideal Electric Dipole Source to a Point Probe

In order to verify the reciprocity theorem in an actual numerical simulation, we set up two simulations, as shown in Fig. 3(a). For setup 1, we place an \hat{x} polarized electric dipole at position $\mathbf{r}_1 = (0, 0, 1)$ cm and a point probe at $\mathbf{r}_2 = (2.5, 3.0, 7.5)$ cm. For setup 2, we put an \hat{z} polarized electric dipole at position \mathbf{r}_2 and a point probe at \mathbf{r}_1 . The background is a homogenous material with relative permittivity of 5 and conductivity of 0.01 S/m; the inner (blue) cuboid is a rectangular object with size of $3 \times 4 \times 5$ cm³ with the relative permittivity 10 and the conductivity 0.1 S/m. Fig. 3(b) shows that the E_z response of setup 1 is the same as the E_x response of setup 2. Through these simulations, the reciprocity of the ideal electric dipole source to a point probe is verified in simulation.

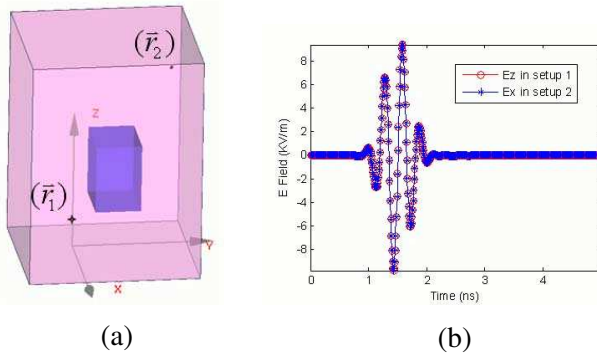


Figure 3. Verification of the reciprocity of an ideal electric dipole source to a point probe in an inhomogeneous medium with a dielectric cube of dimensions $3 \times 4 \times 5$ cm³ centered at (1.0, 1.3, 3.2) m, $\epsilon_r = 10$ and $\sigma = 0.1$ S/m in a homogeneous background with $\epsilon_{rb} = 5$ and $\sigma_b = 0.01$ S/m. (a) Simulation setup with a x -oriented electric dipole at $\mathbf{r}_1 = (0, 0, 1)$ cm and a point probe at $\mathbf{r}_2 = (2.5, 3.0, 7.5)$ cm. (b) Transient E_z response of setup 1 versus transient E_x response of setup 2.

3.2. Verification of the Reciprocity of an Ideal Electric Dipole Source to a Wave Port

Next, we verify the reciprocity between an ideal electric dipole source and a wave port in a Planar Inverted F Antenna (PIFA) placed in medium with $\epsilon_{rb} = 5$ and $\sigma_b = 0.01 \text{ S/m}$. The antenna wave port is extended to air. The configuration is shown in Fig. 4(a), while the PIFA antenna geometry is give in Fig. 4(b). We set up two cases to verify that the voltage response on a wave port is reciprocal to the electric field response at a point probe in simulation. For setup 1, we place an \hat{x} polarized electric dipole at position $\mathbf{r}_1 = (0.5, 0.7, 1.0) \text{ cm}$ and a receiving mode wave port (the red rectangle) on the antenna feeding coax. For setup 2, we put a point probe at \mathbf{r}_1 , and change the wave port as source with the TEM mode in the coax. Except for the wave port of a coaxial cable, the background is a homogenous material with relative permittivity of 5 and conductivity of 0.01 S/m . Fig. 4(c) shows the voltage response on the wave port for setup 1 and the E_x response of setup 2. These two curves agree very well. Through these simulations, we know the voltage response on a wave port is reciprocal to the electric field response at a point probe in numerical simulation.

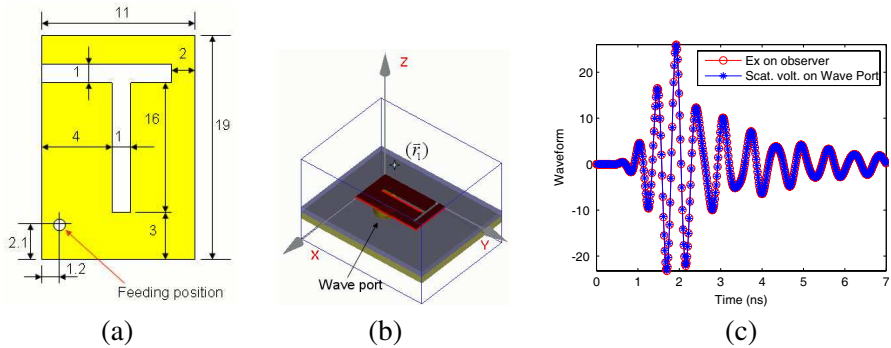


Figure 4. Verification of the reciprocity of an ideal electric dipole source to a wave port in a PIFA antenna placed in a medium with $\epsilon_{rb} = 5$ and $\sigma_b = 0.01 \text{ S/m}$. (a) Simulation setup. (b) Antenna geometry. (c) Transient E_x response of setup 1 versus transient wave port voltage response of setup 2.

3.3. Verification of the Wave Port Green's Function \mathbf{G}_u

Here, we setup an imaging chamber to test the accuracy of the Green's function for a wave port scattered voltage in a non-canonical inhomogeneous background medium. The chamber is sealed by five grounded PCB panels, and only open at the $+y$ direction. There are 8 PIFA fabricated on each side panel, thus totally 32 antennas in the chamber, as shown in Fig. 5(a). Each antenna is fed by a coax as shown in Fig. 4; there is a wave port on the cross-section of each coax. The chamber size is $10 \times 10 \times 10 \text{ cm}^3$, filled with a fluid with relative permittivity of 7.5 and conductivity of 0.01 S/m. A cuboid (size is $4 \times 1.6 \times 2 \text{ cm}^3$) with relative permittivity of 13 and conductivity of 0.1 S/m is placed close to the bottom of the chamber, as shown in Fig. 5(b). The cuboid is meshed by $20 \times 8 \times 10$ cells in forward scattering calculation in Equation (16). In the simulation, there is a point probe at each cell center to record the electric field.

Firstly, we remove the cuboid from the chamber. We record the electric field at each cell center as \mathbf{E}^{inc} . According to the reciprocity theorem, this field is also the vector Green's function $\mathbf{G}_u(\mathbf{r}_2, \mathbf{r}_1)$ from cell center to the wave port. Then we put the cuboid into the chamber and record the electric field at each cell center as the total field \mathbf{E} . Because we know the contrast of the cuboid, we can obtain the induced current at each cell center by $\mathbf{J} = j\omega\epsilon_b\chi\mathbf{E}$, then the scattered voltage at each wave port can be obtained by (16).

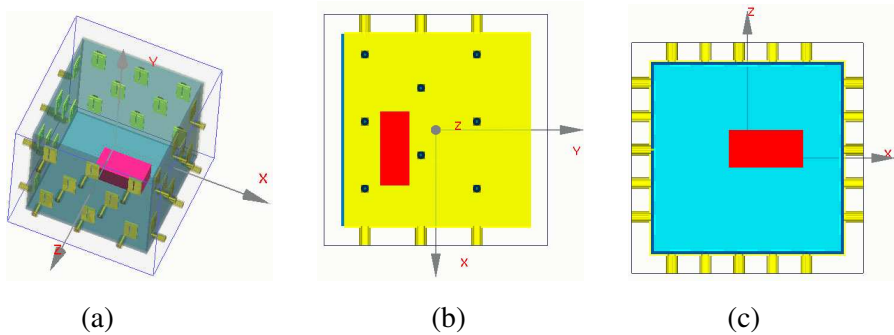


Figure 5. Verification of the vector wave port Green's function $\mathbf{G}_u(\mathbf{r}_2, \mathbf{r}_1)$ for a realistic microwave imaging chamber with 32 PIFA antennas. (a) Simulation setup of the chamber, with each of the four side panels having 8 PIFA antennas given in Fig. 4. The bottom face is PEC, and the top face is open to air. (b) A cuboid in the chamber (size view). (c) A cuboid in the chamber (front view).

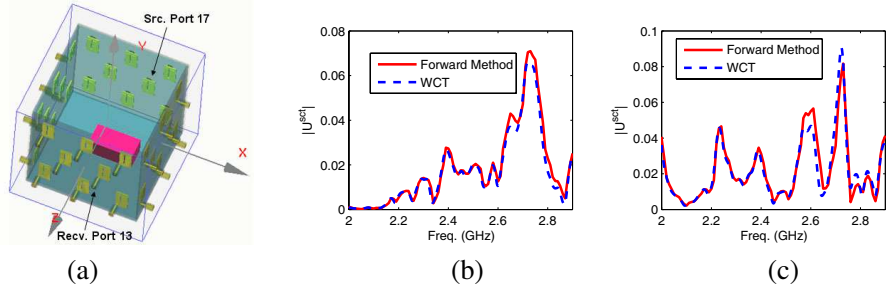


Figure 6. Comparison of scattered voltage at wave ports calculated by the vector wave port Green’s function and by the FDTD method with Wavenology EM for the problem in Fig. 5. (a) Wave ports 17 is used as a source port to calculate the scattered wave port voltage. (b) $|U^{sct}|$ on port 17. (c) $|U^{sct}|$ on port 13.

We calculate the scattered wave port voltage by operating the vector wave port Green’s function on the induced current density given calculated by the FDTD method through Wavenology EM. We then compare this voltage with the FDTD calculation by Wavenology EM. Fig. 6 shows the comparison of the simulated scattered voltage and the reference result by Wavenology EM at each wave port in frequency domain. The result from (16) matches the reference result very well. The small mismatch at the high frequency part is due to the lower meshing density of (10) for (16) in high frequency range (10 sampling points per wavelength at 2.75 GHz). From this test, we know that (16) works well in this complicated antenna array. This verifies the vector wave port Green’s function in this realistic microwave imaging chamber.

3.4. The Scattered Field by DTA in a System with Five PEC Panels

The above examples verify the reciprocity and Green’s functions for inhomogeneous media. Next, we set up a non-canonical inhomogeneous background case to test the accuracy of scattered field calculated by the proposed DTA method combined with the numerical Green’s functions. This case is designed to test a measurement system which employs impedance-matched point dipole probes to measure the field directly. As shown in Fig. 7(a), the background medium contains five PEC panels and two cuboids. The distance between facing PEC panels is 10 cm. The size of each cuboid is $8 \times 8 \times 4 \text{ cm}^3$. The electric properties of all materials are shown in Fig. 7(b). There are 44 probes in the

simulation, as shown in Fig. 7(c), distributed along 4 straight lines, each line having 11 probes. The distance between two adjacent probes along the same line is 8 mm.

The target is a sphere placed at the center of the system (the red sphere shown in Fig. 7(c)), which has a radius of 10 mm, and with $\epsilon_r = 4$ and $\sigma = 0.1 \text{ S/m}$. Fig. 8 shows the scattered electric field at the probes at 2.75 GHz. It shows the scattered field through the DTA method is much better than the Born approximation, even for a sphere with size of $0.34\lambda_{bk_g}$ with contrast $\chi = 1$; the scattered field calculated by the DTA method has 10% relative RMS error compared with the reference full-wave results.

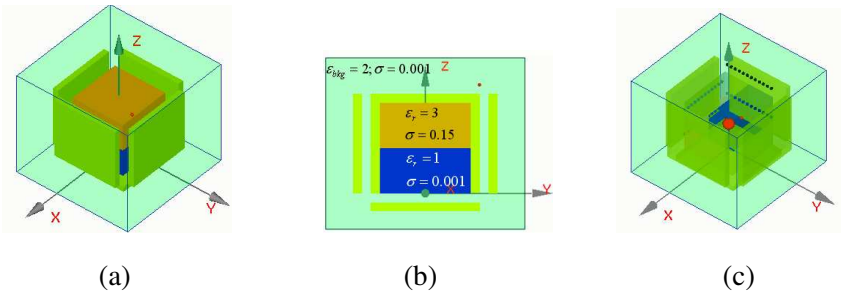


Figure 7. The scattered field by DTA in a system with five PEC panels. (a) Angle view of the simulation setup, where the red dot is the ideal electric dipole source. (b) Cross-section of the case, where for $\epsilon_r = 2$ and $\sigma = 0.001 \text{ S/m}$ for the homogenous material except for the PEC and cuboids; for the top cuboid, $\epsilon_r = 3$ and $\sigma = 0.15 \text{ S/m}$; for bottom cuboid, $\epsilon_r = 1$ and $\sigma = 0.0001 \text{ S/m}$. (c) The point probes in the simulation (dark dots), the red sphere ($r = 10 \text{ mm}$) is the target.

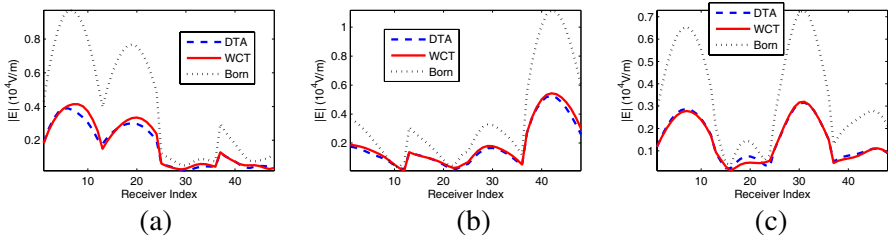


Figure 8. Comparison of the scattered electric field for the system in Fig. 7 calculated by DTA, Born approximation, and Wavenology EM for (a) $|E_x^{sct}|$, (b) $|E_y^{sct}|$, and (c) $|E_z^{sct}|$.

3.5. The Scattered Voltage from Two Cubes by DTA in a Chamber

In this example, we study a microwave imaging chamber to test the accuracy of the scattered voltage at wave ports by the DTA method combined with the numerical Green's function. The chamber is sealed by 5 PCB panels, only open at the $+z$ direction. Similar to the case in Fig. 6, with 8 PIFA antennas fabricated on each side panel, thus totally 32 antennas. Each antenna is fed by a wave port on the cross-section of the coax. The chamber size is $10 \times 10 \times 10 \text{ cm}^3$, filled with a fluid having relative permittivity of 5 and conductivity of 0.01 S/m . Two cuboids of dimensions $4 \times 4 \times 4 \text{ cm}^3$ are placed in the chamber, as shown in Fig. 9. The top cuboid has relative permittivity of 8 and conductivity of 0.2 S/m . The bottom cuboid has relative permittivity of 6 and conductivity of 0.02 S/m . The forward computation domain is the bounding box of the two cuboids, meshed by $12 \times 12 \times 12$ cells.

Figure 10 shows the scattered voltage on 32 probes at frequency 2.75 GHz when the source port is port 17. The scattered voltage results calculated by the DTA method agree well with the reference full-wave results, with 15% relative RMS error.

3.6. The Scattered Voltage from Eight Small Cubes by DTA in a Chamber

Finally, we examine the DTA accuracy for the scattering from multiple small objects. In this case, 8 cubes (each with dimensions $12 \times 12 \times 12 \text{ mm}^3$) are placed in two layers in the computation domain. The

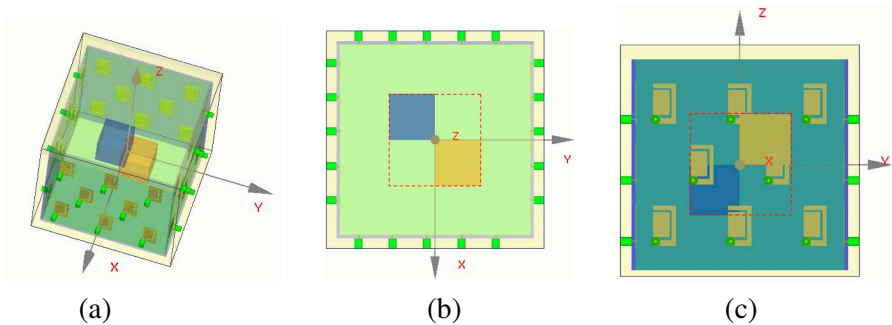


Figure 9. Two cubes in an imaging chamber. (a) Angle view of the configuration. (b) Top view of the configuration, with the dashed line indicating the forward simulation domain. (c) Side view of the configuration.

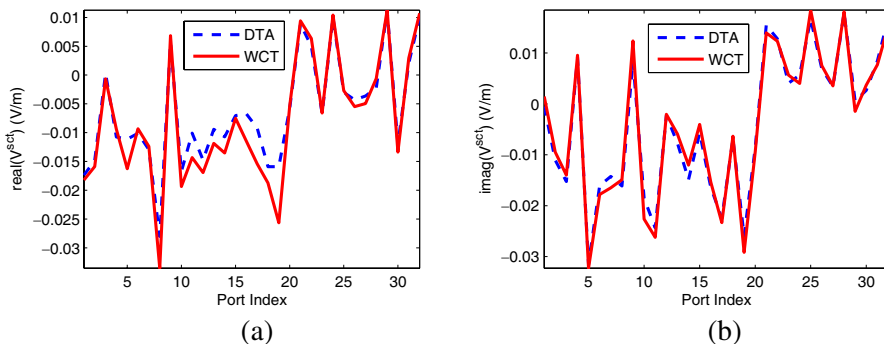


Figure 10. The calculated scattered voltage from the two cubes in a microwave imaging chamber in Fig. 9. Comparison of (a) the real part, and (b) imaginary part of the scattered voltage with the reference full-wave results obtained by Wavenology EM.

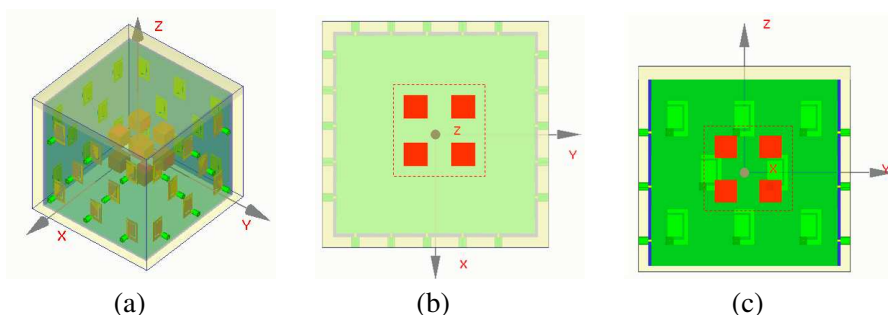


Figure 11. Scattered voltages from eight small cubes in the microwave imaging chamber. (a) Angle view of the simulation setup. (b) Top view of the configuration with the red dashed line indicating the computational domain. (c) The side view of the configuration.

positions of these 8 cubes are shown in Fig. 11, with the distance between any adjacent cells being $\lambda/4$ in the background fluid at 2.7 GHz; and the size of cube is $\lambda/4$ also. All cubes have the same electric properties of a relative permittivity 10 and conductivity 0.2 S/m.

Figure 12 shows the scattered voltage at the 32 wave ports at frequency 2.75 GHz (source port is port 17). The scattered voltage through the DTA method has 18% relative RMS error compared with the reference full-wave results.

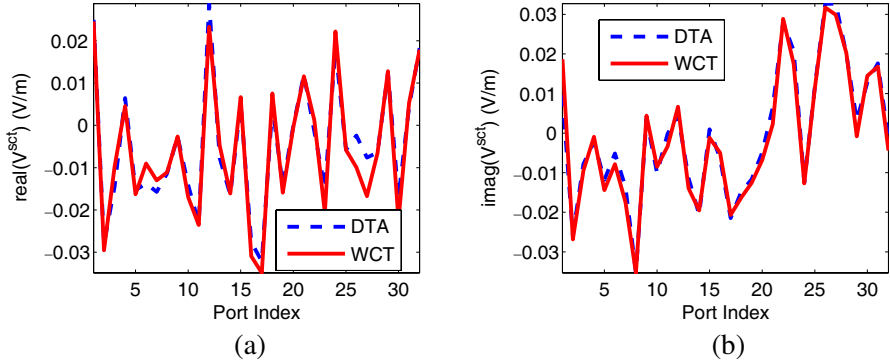


Figure 12. Comparison of the DTA calculated scattered voltage with Wavenology EM for the (a) real part and (b) imaginary part of the scattered voltage at the 32 ports.

From the last two cases, it is shown that our proposed method works well in a complicated non-canonical inhomogeneous background. The DTA method combined with the electric field-voltage conversion can provide acceptable scattering field results for such complicated configurations. Therefore, we expect that this approximate DTA solver will be useful for both the forward and inverse scattering computation in microwave imaging.

4. CONCLUSION

We demonstrate the first application of the Diagonal Tensor Approximation to calculate the scattered fields from arbitrary objects in a non-canonical inhomogeneous background. This extends the application domain of the DTA from previous canonical background media (such as homogeneous and layered-medium background) to arbitrary inhomogeneous background media. The method relies on the numerical computation of the Green's functions. We take advantage of the symmetry of the configuration and the reciprocal property of the Green's function to reduce the number of the simulation cases. Furthermore, we develop the necessary formulation to relate the wave port voltage at an antenna to the fields in the computation domain. Extensive numerical results show that this method can accurately obtain the scattered fields from arbitrary objects in a non-canonical inhomogeneous background. Future work will apply this method to perform inverse scattering computation for microwave imaging.

REFERENCES

1. Harrington, R. F., *Field Computation by Moment Method*, R. E. Krieger, Editor, Malabar, FL, 1968.
2. Born, M. and E. Wolf, *Principles of Optics*, Pergamon, New York, 1980.
3. Habashy, T. M., R. W. Groom, and B. R. Spies, "Beyond the born and Rytov approximations. A nonlinear approach to electromagnetic scattering," *J. Geophys. Res.*, Vol. 98, 1759–1775, 1993.
4. Torres-Verdin, C. and T. M. Habashy, "Rapid 2.5-D forward modeling and inversion via a new nonlinear scattering approximation," *Radio Sci.*, Vol. 29, 1051–1079, 1994.
5. Zhang, M. S. and S. Fang, "Three-dimensional quasi-linear electromagnetic inversion," *Radio Sci.*, Vol. 31, 741–754, 1996.
6. Zhang, M. S. and S. Fang, "Quasi-linear approximation in 3-D electromagnetic modeling," *Geophysics*, Vol. 61, 646–665, 1996.
7. Zhang, M. S. and S. Fang, "Quasi-linear series in three-dimensional electromagnetic modeling," *Radio Sci.*, Vol. 32, 2167–2188, 1997.
8. Song, L. P. and Q. H. Liu, "Fast three-dimensional electromagnetic nonlinear inversion in layered media with a novel scattering approximation," *Inverse Problems*, Vol. 20, 171–194, 2004.
9. Song, L.-P. and Q. H. Liu, "A new approximation to three-dimensional electromagnetic scattering," *IEEE Geosci. Remote Sensing Lett.*, Vol. 2, No. 2, 238–242, April 2005.
10. Zhang, Z. Q. and Q. H. Liu, "Two nonlinear inverse methods for electromagnetic induction measurements," *IEEE Trans. Geosci. Remote Sensing*, Vol. 39, No. 6, 1331–1339, June 2001.
11. Cui, T. J., W. C. Chew, A. A. Alaeddin, and Y. H. Zhang, "Fast-forward solvers for the low-frequency detection of buried dielectric objects," *IEEE Trans. Geosci. Remote Sensing*, Vol. 41, 2026–2036, 2003.
12. Miller, E. L. and A. S. Willsky, "Wavelet-based methods for the nonlinear inverse scattering problem using the extended born approximation," *Radio Sci.*, Vol. 31, 51–65, 1996.
13. Tseng, H. W., K. H. Lee, and A. Becker, "3D interpretation of electromagnetic data using a modified extended Born approximation," *Geophysics*, Vol. 68, 127–137, 2003.
14. Liu, Q. H., Z. Q. Zhang, T. T. Wang, J. A. Bryan, G. A. Ybarra, L. W. Nolte, and W. T. Joines, "Active microwave imaging I: 2-D forward and inverse scattering methods," *IEEE Trans. Microwave*

- Theory Tech.*, Vol. 50, 123–133, January 2002.
15. Yu, C., M. Q. Yuan, J. Stang, E. Bresslour, R. T. George, G. A. Ybarra, W. T. Joines, and Q. H. Liu, “Active microwave imaging II: 3-D system prototype and image reconstruction from experimental data,” *IEEE Trans. Microwave Theory Tech.*, Vol. 56, No. 4, 991–1000, 2008.
 16. Li, F., Q. H. Liu, and L.-P. Song, “Three-dimensional reconstruction of objects buried in layered media using Born and distorted Born iterative methods,” *IEEE Geosci. Remote Sensing Lett.*, Vol. 1, No. 2, 107–111, 2004.
 17. Abubakar, A., P. M. van den Berg, and J. T. Fokkema, “Towards non-linear inversion for characterization of time-lapse phenomena through numerical modeling,” *Geophys. Prospect.*, Vol. 51, 285–293, 2003.
 18. Yuan, M. Q., C. Yu., J. P. Stang, R. T. George, G. A. Ybarra, W. T. Joines, and Q. H. Liu, “Experiments and simulations of an antenna array for biomedical microwave imaging applications,” *URSI Meeting*, San Diego, CA, July 2008.
 19. Yu, C., M. Q. Yuan, J. P. Stang, J. E. Bresslour, R. T. George, G. A. Ybarra, W. T. Joines, and Q. H. Liu, “Active microwave imaging II: 3-D system prototype and image reconstruction from experimental data,” *IEEE Trans. Microwave Theory Tech.*, Vol. 56, No. 4, 991–1000, 2008.
 20. Yu, C., M. Q. Yuan, and Q. H. Liu, “Reconstruction of 3D objects from multi-frequency experimental data with a fast DBIM-BCGS method,” *Inverse Problems*, Vol. 25, Feb. 2009.
 21. Gelius, L.-J., “Electromagnetic scattering approximations revisited,” *Progress In Electromagnetics Research*, Vol. 76, 75–94, 2007.
 22. Yu, C., M. Q. Yuan, Y. Zhang, J. Stang, R. T. George, G. A. Ybarra, W. T. Joines, and Q. H. Liu, “Microwave imaging in layered media: 3-D image reconstruction from experimental data,” *IEEE Trans. Antennas Propagat.*, Vol. 58, No. 2, February 2010.
 23. Hernandez-Lopez, M. A. and M. Quintillan-Gonzalez, “Coupling and footprint numerical features for a bow-tie antenna array,” *Journal of Electromagnetic Waves and Applications*, Vol. 19, No. 6, 779–794, 2005.
 24. Guo, B., Y. Wang, J. Li, P. Stoica, and R. Wu, “Microwave imaging via adaptive beamforming methods for breast cancer detection,” *Journal of Electromagnetic Waves and Applications*, Vol. 20, No. 1, 53–63, 2006.
 25. Yu, J., M. Yuan, and Q. H. Liu, “A wideband half oval

- patch antenna for breast imaging,” *Progress In Electromagnetics Research*, Vol. 98, 1–13, 2009.
26. Gwarek, W. and M. Celuch-Marcysiak, “Wide-band S -parameter extraction form FDTD simulations for propagating and evanescent modes in inhomogenous guides,” *IEEE Trans. Microwave Theory Tech.*, Vol. 51, No. 8, 1920–1928, August 2003.
 27. Chew, W. C. and Q. H. Liu, “Inversion of induction tool measurements using the distorted Born iterative method and CG-FFHT,” *IEEE Trans. Geosci. Remote Sensing*, Vol. 32, 878–884, July 1994.
 28. Newman, G. A., “Cross well electromagnetic inversion using integral and differential equations,” *Geophysics*, Vol. 60, 899–910, 1995.
 29. Torres-Verdin, C. and T. M. Habashy, “A two-step linear inversion of two-dimensional electrical conductivity,” *IEEE Trans. Antennas Propagat.*, Vol. 43, 405–415, 1995.
 30. Van den Berg, P. M. and M. van der Horst, “Nonlinear inversion in induction logging using the modified gradient method,” *Radio Sci.*, Vol. 30, 1355–1369, 1995.
 31. Howard, Jr., A. Q., W. C. Chew, and M. C. Moldoveanu, “A new correction to the born approximation,” *IEEE Trans. Geosci. Remote Sensing*, Vol. 28, 394–399, May 1990.